ISSN 0915-633X

NATIONAL INSTITUTE FOR FUSION SCIENCE

Simulation Study of Toroidal Phase-Locking Mechanism in Reversed-Field Pinch Plasma

K. Kusano, T. Tamano and T. Sato

(Received – Jan. 17, 1991)

NIFS-78 Feb. 1991

RESEARCH REPORT
NIFS Series

NAGOYA, JAPAN

SIMULATION STUDY OF TOROIDAL PHASE-LOCKING MECHANISM IN REVERSED-FIELD PINCH PLASMA

Kanya KUSANO, Teruo TAMANO† and Tetsuya SATO‡

Department of Materials Science, Faculty of Science,
Hiroshima University, Hiroshima 730, Japan
†*General Atomics, San Diego, CA 92138, U.S.A.*
‡*National Institute for Fusion Science, Nagoya 464-01, Japan*

Abstract

The toroidal phase locking process of kink modes in the reversed-field pinch (RFP) plasma is investigated in detail by means of the magnetohydrodynamic (MHD) simulation. The physical mechanism of phase locking is clarified. The most dominant two linearly unstable kink modes rule over the evolution of other kink modes whereby phase locking takes place. It is confirmed that the phase locking process is not a special phenomenon subject to the resistive boundary condition, but a common feature of the MHD relaxation process in the RFP. The relation between the phase locking and MHD relaxation processes is briefly discussed.

Key Words: RFP, PHASE LOCKING, MHD SIMULATION, MHD RELAXATION, KINK INSTABILITY

1 Introduction

It is widely recognized that the reversed-field pinch (RFP) plasma involves many types of nonlinear interaction. The OHTE experiment has recently found [1] a very curious, new type phenomenon. It is a toroidally localized kink instability, which is called "slinky mode". It is experimentally shown that the slinky mode is a result of phase locking of several internal kink modes.

Recently Schnack and Ortolani succeeded in demonstrating the phase locking phenomenon of RFP by using a new code providing the resistive shell boundary [2]. In this respect they mentioned that not only in the case of the resistive shell boundary but also in the case of the perfectly conducting boundary the similar phase locking would take place. This suggests that the phase locking of kink modes may not be a special characteristic subject to the resistive boundary but a general feature in nonlinear evolution of RFP.

In spite of their efforts, however, the physical mechanism of the phase locking process is not explained satisfactorily. The purpose of this paper is to give a theoretical interpretation for the phase locking mechanism. In this paper we first show, using a magnetohydrodynamic (MHD) simulation, that phase locking occurs even for the case of perfectly conducting boundary (Section 3). Then we go on to study the question about the toroidal location where phase locking takes place (Section 4). This question will lead us to the physical interpretation of the phase locking mechanism (Section 4). The numerical model is explained in Section 2. In Section 5, we will summarize our principal conclusions.

2 Simulation Model

To simulate the phase locking process of RFP, we use a Fourier-expanded MHD code which is the same code used in the previous paper [3]. A periodic cylindrical geometry is adopted and the physical variables are decomposed into the poloidal (m) and the toroidal (n) mode components, *i.e.*

$$f(r,\theta,z) = \sum_{m,n} \tilde{f}\,(r,m;n) \exp i(m\theta - nz/R). \tag{1}$$

The aspect ratio of the cylindrical torus is $5/\pi$. The azimuthal (θ) and axial (z) derivatives are calculated in the complex Fourier space, but the radial one is approximated by a two point central difference. The number of the radial grid elements is 51. The Runge-Kutta-Gill time advancing method is used.

The basic equations and the normalization except for the magnetic field are the same as those in the previous paper (see Eqs. (2) to (6) in Ref.[3]). The normalizing factor for the magnetic field B_0 is chosen to be the initial toroidal magnetic field at the axis $B_z(r=0)$. The resistivity η and the viscosity ν are fixed to 10^{-4}.

The initial condition is composed of a force-free equilibrium and kink perturbations given by

$$\begin{pmatrix} \mathbf{V}_{initial} \\ \mathbf{B}_{initial} \end{pmatrix} = \begin{pmatrix} 0 \\ \mathbf{B}_{force-free} \end{pmatrix} + \begin{pmatrix} \mathbf{v}_0 \\ \mathbf{b}_0 \end{pmatrix}. \tag{2}$$

The equilibrium $\mathbf{B}_{force-free}$ is similar to that used in the previous paper [3]. It is specified by the following profile of the ratio λ between the magnetic field B and the current J,

$$\lambda = \frac{\mathbf{J}\cdot\mathbf{B}}{\mathrm{B}^2} = \lambda_0\{\frac{\cos\pi r + 1}{2}\}^{\zeta}. \tag{3}$$

In our initial equilibrium, λ_0 and ζ are chosen to be 6.57 and 2, respectively. This is an unstable equilibrium against the kink mode instability for $n = 2$ to 9. Figure 1 shows the linear growth rate for each mode, and we can see that the mode (1;5) is the most unstable mode. The q-value at the central axis is 0.19, and hence the mode (1;5) is almost the on-axis mode.

The perturbations, $\mathbf{v}_0$ and $\mathbf{b}_0$, are given by the linear eigenfunctions and an additional phase at the origin, ϕ_n $(-\pi < \phi_n < \pi)$, *i.e.*

$$\begin{pmatrix} \mathbf{v}_0 \\ \mathbf{b}_0 \end{pmatrix} = \sum_n \begin{pmatrix} \tilde{\mathbf{v}}_{eigen-function}(r,n) \\ \tilde{\mathbf{b}}_{eigen-function}(r,n) \end{pmatrix} \exp i(\theta - nz/R + \phi_n), \tag{4}$$

where the phase distribution $\{\phi_n : n = 2 \text{ to } 9\}$ is given by a random number. In eq.(4), the summation is over all unstable modes ($n = 2$ to 9). The relative amplitude of the perturbation for each mode to the equilibrium is 10^{-4}.

The boundary conditions are given by

$$\mathbf{V} = 0, \tag{5}$$

$$B_r = 0, \tag{6}$$

$$\mathbf{E} = 0. \tag{7}$$

Condition (5) is the condition of the standard rigid boundary for viscous fluid. Conditions (6) and (7) are the conditions of the perfectly conducting boundary. In this paper, in order to confirm that the phase locking process is a general feature of RFP dynamics rather than a special instability in the thin shell (resistive shell) device, we employ the perfectly conducting boundary condition.

Simulation runs are performed for two cases, Case 1 and Case 2 which are given in Table I. Since the principal modes in the MHD relaxation process are the low m modes [3], this mode system may be sufficient to simulate the basic nonlinear processes in the RFP plasma. The difference between Cases 1 and 2 is that the most unstable kink mode, $(m; n) = (1; 5)$, is removed in Case 2.

3 Simulation Results

First of all, let us examine Case 1, using the same diagnostic formats as those used in the OHTE experiment [1]. Figure 2 shows the typical simulation results for three different times, namely, at $t = 10$, 28 and 40 τ_A (Alfvén time). The top and the third subsets, (a) and (c), show the normalized toroidal mode profiles of B_r, *i.e.*

$$\beta(z) \equiv \mathrm{Re}\{\frac{\tilde{B}_r(r = 0.9, m = 1; n)}{|\tilde{B}_r|} \exp(-inz/R)\},$$

for the low n ($n = 1$ to 10) and for the high n ($n = 11$ to 20) modes, respectively. The second and fourth subsets, (b) and (d), represent the dispersion σ of the phase distributions for the low n and the high n modes, respectively. The bottom subset (e) shows the real profile of $B_r(r = 0.9, \theta = 0, z)$. The dispersion of the phase distribution σ is calculated by

$$\sigma(z) = \sqrt{\frac{\sum_n \{\varphi_n(z) - \overline{\varphi}(z)\}^2}{N_{sum}}}, \tag{8}$$

where

$$\varphi_n(z) = \pi^{-1} \tan^{-1} \frac{\mathrm{Im}\{\tilde{B}_r(r = 0.9, m = 1, n) \exp(-inz/R)\}}{\mathrm{Re}\{\tilde{B}_r(r = 0.9, m = 1, n) \exp(-inz/R)\}}, \tag{9}$$

and

$$\overline{\varphi}(z) = \frac{\sum_n \varphi_n(z)}{N_{sum}}. \tag{10}$$

In eqs.(8) and (10), N_{sum} is the number of the modes which contribute to the summation $\sum_n$. In eq.(9), the phase $\varphi_n(z)$ has a value in the range

$$\xi(z) \geq \varphi_n(z) \geq \xi(z) + 2,$$

and $\xi(z)$ is adjusted so that $\sigma(z)$ has the smallest value. So, the dispersion σ can be a good indicator for the phase locking. Phase locking becomes more complete, as the dispersion σ becomes smaller.

We can see that at $t = 10\tau_A$ the phase distribution is extremely random both for the low n and high n modes. It obviously reflects the initial random phase distribution of the perturbation modes. After some time has elapsed, the phases of the high n modes are locked at a certain toroidal location, *i.e.*, $z = 1.1$ at $t = 28\tau_A$. Note that the dispersion σ for the high n modes has a clear minimum at this point, whose value is 0.03. The real B_r profile is locally perturbed around there. Therefore, phase locking, *'slinky mode'*, appears. However, phase locking disappears at $t = 40\tau_A$ and the phase distribution becomes random again. On the other hand, the low n modes do not exhibit such a clear phase locking as obtained for the high n modes at any time.

Let us examine the phase evolution for each mode. In Fig. 3, the time history of the phase φ_n for each mode seen at the point $z = 1.1$, where the σ has a minimum in time and space, is plotted along with the evolution of the spatially minimum σ. In the linear phase, before $t \cong 10\tau_A$, the phase of each mode is almost fixed to the initial phase. In the period $10\tau_A < t < 20\tau_A$, however, the phases are greatly altered by nonlinear coupling among the modes. As a result of the nonlinear evolution, all high n modes have the same phase at $t \cong 20\tau_A$, and phase locking starts. Here we should notice that the modes attributing to the phase locking are not only the high n modes ($n \geq 11$) but also the middle n modes (n=5, 7, 8, 9, 10). (The locked modes are bundled by the circle with the arrow.) Remember that the initial on-axis mode is the $n = 5$ kink mode. Therefore, the locked modes are only the internal kink modes. These results are consistent with the results of the experiment [1] and the previous simulation [2]. The phase locking continues until about $t = 30\tau_A$. For $t > 30\tau_A$, the phase locking is lost and the distribution becomes random again.

From the results shown in Figs. 2 and 3, it is confirmed that the phase locking process can take place for the case with perfectly conducting boundary condition.

Therefore it is not a special phenomenon subject to the resistive boundary condition.

4 Discussion

Now, let us advance to the study of the physical mechanism of the phase locking process. The key-question addressed is what decides the toroidal location where the phases locking appears. The answer is that the phase distribution of the most unstable two kink modes in the linear phase determines the location.

In order to prove this answer, we carry out the twenty six different simulations, those have different random phase distributions, $\{\phi_n\}$ in eq.(4). However, all other parameters except ϕ_n are the same as those in the simulation shown above. Figure 4 shows the relation between two toroidal locations $z_{p.l.}$ and z_{n_1/n_2} for the twenty six simulations. The $z_{p.l.}$ is the location where the phase locking takes place, *i.e.* the location where the dispersion σ for the high n modes has the smallest value in space and time. The z_{n_1/n_2} is the location where the two kink modes, $(m;n) = (1,n_1)$ and $(1,n_2)$, initially have the same phase, that is given by

$$z_{n_1/n_2} = R\frac{\phi_{n_1} - \phi_{n_2}}{n_1 - n_2}. \tag{11}$$

Figures 4 (a) and (b) are for $n_1/n_2 = 4/5$ and $5/6$, respectively. We can see that there is a good correlation between the locations $z_{p.l.}$ and $z_{4/5}$. In fact, the location $z_{p.l.}$ is distributed around the line,

$$z_{p.l.} = (z_{4/5} + \pi R) \bmod (2\pi R). \tag{12}$$

On the other hand, the relation between $z_{p.l.}$ and $z_{5/6}$ is not well correlated, as is shown in Fig. 4 (b). Actually we cannot find that the other mode sets except $n_1/n_2 = 4/5$ have a systematic relation with the location $z_{p.l.}$.

As shown in Fig. 1, the modes (1;4) and (1;5) have the largest linear growth rates in the initial state. Not only in the linear phase but also in the nonlinear phase, they are the most dominant modes. Figure 5 shows the history of the magnetic energy for the initially unstable modes. We can see that each mode grows exponentially with its linear growth rate in the linear phase ($0 < t < 10\tau_A$). Because of the large linear growth rates, the amplitudes of the modes (1;4) and (1;5) quickly grow. In the period

$10\tau_A < t < 20\tau_A$, although these modes exhibit gradual saturation, the modes (1;5) and (1;4) remain the dominant and the second dominant. However, the amplitudes for these modes start to decrease after about $t = 20\tau_A$, and at $t = 27\tau_A$ the mode (1;5) gives up being the most dominant mode. It is worth to point out that phase locking appears when the magnetic energy for the modes (1;5) and (1;4) are maximized, and that the phase locking continues as long as the mode (1;5) is dominant.

These results in Figs. 4 and 5 indicate that the most dominant two kink modes govern the other modes whereby they are phase locked. It is also indicated that when the leading modes lose their influences, the phase locking process terminates. In order to examine this hypothesis, we carry out another type of simulation, namely, Case 2. In Case 2 simulation, only the mode (1;5), that seems to be the leading mode for phase locking, is removed from the simulation system. Figures 6 (a) and (b) are the histograms for the minimum dispersion σ in the different twenty six simulation runs for Cases 1 and 2, respectively. In the both simulations, the initial phase distributions $\{\phi_n\}$ are determined by different random numbers. Figure 6 (a) is the result taken from the same simulation runs as shown in Fig.4. We can see in Fig.6 (a) that the most runs for Case 1 have smaller dispersion than 0.05. This means that the clear phase locking process appears irrespective of the initial phase distribution. On the other hand, as shown in Fig. 6 (b), the peak of the minimum dispersion distribution shifts to the range 0.1 to 0.15 for Case 2. Furthermore, the distribution becomes broader in comparison with Case 1. These results indicate that the removal of the most dominant mode (1;5) makes phase locking less clear, which supports our hypothesis given in the beginning of this paragraph.

Now, let us show more directly the fact that the most dominant modes govern the other kink modes. In Fig. 7, the amplitude of each coupling term in the nonlinear phase (at $t = 15\tau_A$) is plotted. This diagram shows the amplitude of the nonlinear coupling between the modes $(m'; n')$ and $(m - m'; n - n')$, which affects the evolution of the mode $(m; n)$. The abscissa and the ordinate correspond to the mode $(m; n)$ and the mode $(m'; n')$, respectively. The size of each diamond plotted in the diagram is proportional to the amplitude of nonlinear coupling Ξ, that is given by

$$\Xi(m; n, m'; n') \equiv |\mathrm{rot}\{\tilde{\mathbf{V}}(r = 0.9, m'; n') \times \tilde{\mathbf{B}}(r = 0.9, m - m'; n - n')\}_r|. \qquad (13)$$

The size of the diamond for the modes $(m;n)$ and $(m';n')$ is normalized by the largest coupling term $\Xi_{max}(m;n)$,

$$\Xi_{max}(m;n) \geq \Xi(m;n,m';n') \quad \text{for any } (m';n'),$$

which is scaled as the unit. Only the three largest couplings are plotted for each mode $(m;n)$. Hence, the position of the unit scale diamond represents the most influential coupling on the mode $(m;n)$.

First, we can see that for the low n kink modes the most dominant coupling is located on the line A, while the dominant coupling for the high n modes is located off the line. The coupling on the line A is the coupling with itself, *i.e.* the linear coupling. Hence it means that the low n kink modes are almost governed by the linear response, while the high n kink modes are affected mainly by the nonlinear coupling.[1] The second important result is that most of the diamonds are distributed inside of the two triangle zones surrounded by the lines A and B. The coupling on the line B is the coupling with the mode (1;5), that is the key-mode in the phase locking process. It means therefore that the kink modes for $n > 5$ are governed by the lower n mode than itself. On the other hand, the modes for $n < 5$ are affected by the higher n mode than itself. Eventually, all the kink modes are more or less affected by the mode (1;5). However, the effect of the nonlinear coupling on the low n modes is not so influential in comparison with the linear effect. This fact explains that the lower n modes than the most dominant kink mode ($n = 5$) can not contribute to phase locking. Furthermore, it is worthwhile to point out that the most dominant kink mode is almost usually the on-axis mode. (For instance, see Fig.2 in Ref.[4].) Therefore, only the internal kink modes, that have a higher n number than the on-axis mode, can attribute to the phase locking process as observed both in the experiments and the simulations.

These simulation results strongly support our hypothesis, so we can conclude that phase locking takes place through a nonlinear coupling process that the most dominant two kink modes rule over the evolution of the other kink modes. We can easily understand this conclusion, if we notice the following fact: When there are only two

[1]This fact does not mean that any low n modes are linearly unstable, because the coupling amplitude Ξ is given by the absolute value in eq.(13). Even if the mode is linearly stable, the large linear reaction against the nonlinear perturbation gives the large Ξ on the line A in Fig.7.

perturbation modes in the initial state, all other modes induced from these modes have the same phase as that of the initial two modes at a point where the initial two modes have the same phase.[2] Therefore, we can regard the phase locking to be the result of a nonlinear process, in which one coupling overcomes the other coupling processes.

In the OHTE experiment, it was observed that the two modes were first locked simultaneously and then the other internal kink modes join the phase locking (see Fig.5 in Ref.[1]). The first locked two kink modes (n = 10 and 11 in OHTE experiment) have the helicity m/n corresponding to the q-value on the axis. This experimental observation is consistent with our result, and the first locked modes correspond to the leading modes for the phase locking.

Quite recently, it is found that two kink modes become unstable in the self-sustainment process of the RFP configuration [3]. The nonlinear coupling between these unstable kink modes effectively reproduces the reversed field and introduces the MHD relaxation process. Note that the nonlinear coupling between the most unstable kink modes is also a key-process of phase locking. In fact, it is observed in simulations and experiments [1] that the plasma quickly approaches the Taylar's relaxed state through the phase locking process. Therefore, all RFP plasma accompanied by the MHD relaxation must have a tendency that the phases are locked in the relaxation process. The fact that the phase locking process has not yet been observed in the experiments of the conducting boundary might be due to the stabilizing effect of the boundary. The detailed linear analysis for the kink mode predicts that replacing the conducting boundary by the resistive one greatly enhances the linear growth rate of the kink instability [5,6]. In the phase locking process, the leading modes must have large growth rates whereby they can rule over the other modes. It is likely that the enhancement of the growth rate under the resistive boundary makes the phase locking process clearer. Actually, in our simulation study there is a tendency that phase locking appears more easily as the initial equilibrium is more unstable.

[2]It is mathematically proved in Appendix A.

5 Summary

In this paper, we have in detail investigated the phase locking process in the RFP. Our findings are summarized as follows:

1. Phase locking can take place under the perfectly conducting boundary condition. Hence, it is not a special phenomenon subject to the resistive boundary, but is a common feature in the RFP dynamics.

2. Phase locking takes place at the location where the most dominant two kink modes have the same phase.

3. Phase locking takes place through the process, in which the nonlinear coupling between the most dominant two kink modes rules over the dynamics of the other mode. Therefore, it terminates when the ruling modes die.

Finally, we can conclude that a few kink modes control the almost entire evolution in the RFP dynamics during the MHD relaxation and phase locking processes.

A Appendix

We can easily prove that when there are only two perturbation modes, the phases of any modes driven by these two modes are always locked. Let us assume that the initial state includes only the equilibrium component ($\mathbf{B}_0$) and the two perturbation modes ($\mathbf{V}_1$, $\mathbf{B}_1$) and ($\mathbf{V}_2$, $\mathbf{B}_2$), *i.e.*

$$\begin{aligned} \mathbf{V} &= (\mathrm{V}_{r1}, i\mathrm{V}_{\theta 1}, i\mathrm{V}_{z1}) \exp i(m_1\theta - n_1 z/R + \phi_1) \\ &+ (\mathrm{V}_{r2}, i\mathrm{V}_{\theta 2}, i\mathrm{V}_{z2}) \exp i(m_2\theta - n_2 z/R + \phi_2), \end{aligned} \tag{14}$$

$$\begin{aligned} \mathbf{B} &= (0, \mathrm{B}_{\theta 0}, \mathrm{B}_{z0}) \\ &+ (i\mathrm{B}_{r1}, \mathrm{B}_{\theta 1}, \mathrm{B}_{z1}) \exp i(m_1\theta - n_1 z/R + \phi_1) \\ &+ (i\mathrm{B}_{r2}, \mathrm{B}_{\theta 2}, \mathrm{B}_{z2}) \exp i(m_2\theta - n_2 z/R + \phi_2), \end{aligned} \tag{15}$$

where the variables $\mathrm{V}_{\xi i}$ and $\mathrm{B}_{\xi i}$ ($\xi = r, \theta, z$, and $i = 1, 2$) are real functions of radius only. Because the phases ϕ_1 and ϕ_2 are included, the equations (14) and (15) do not

lose a generality. The poloidal and the toroidal coordinates are periodic in the torus system, hence there is a freedom to choose the origin of the coordinates θ and z at any place. For Convenience, we put the origin at the place where the phases of two perturbation modes are equal to zero. Namely, the coordinates θ and z in equations (14) and (15) are translated into $\theta - \theta_0$ and $z - z_0$, where

$$\theta_0 = \frac{n_1\phi_2 - n_2\phi_1}{m_1 n_2 - m_2 n_1} \tag{16}$$

$$z_0 = \frac{m_1\phi_2 - m_2\phi_1}{m_1 n_2 - m_2 n_1} R. \tag{17}$$

Through this translation, the phases ϕ_1 and ϕ_2 in equations (14) and (15) are vanished without losing a generality. According to the definition of the phase φ, that is given by (9), the phases of the initial two modes $\varphi = \pm 1/2$ at the origin.

Now, the third mode $(\mathbf{V}_3, \mathbf{B}_3)$ is driven by the nonlinear coupling between the modes $(\mathbf{V}_1, \mathbf{B}_1)$ and $(\mathbf{V}_2, \mathbf{B}_2)$, that mode number $(m_3, n_3) = (m_1 + m_2, n_1 + n_2)$. The third mode $(\mathbf{V}_3, \mathbf{B}_3)$ is governed by the equations

$$\frac{\partial \mathbf{V}_3}{\partial t} = \sum_{(i,j)=(1,2),\,(2,1)} \{-(\mathbf{V}_i \cdot \Delta)\mathbf{V}_j + \rho^{-1}\mathbf{J}_i \times \mathbf{B}_j\}, \tag{18}$$

$$\frac{\partial \mathbf{B}_3}{\partial t} = \sum_{(i,j)=(1,2),\,(2,1)} \mathrm{rot}(\mathbf{V}_i \times \mathbf{B}_j), \tag{19}$$

where

$$\begin{aligned}(\mathbf{V}_i \cdot \Delta)\mathbf{V}_j = (\ & \{\ V_{ri}\tfrac{\partial V_{rj}}{\partial r} - \tfrac{m_j}{r}V_{\theta i}V_{rj} + \tfrac{n_j}{R}V_{zi}V_{rj} + \tfrac{1}{r}V_{\theta i}V_{\theta j}\},\\ & i\{\ V_{ri}\tfrac{\partial V_{\theta j}}{\partial r} - \tfrac{m_j}{r}V_{\theta i}V_{\theta j} + \tfrac{n_j}{R}V_{zi}V_{\theta j} + \tfrac{1}{r}V_{\theta i}V_{rj}\},\\ & i\{\ V_{ri}\tfrac{\partial V_{zj}}{\partial r} - \tfrac{m_j}{r}V_{\theta i}V_{zj} + \tfrac{n_j}{R}V_{zi}V_{zj}\ \})\exp i(m_3\theta - \tfrac{n_3}{R}z),\end{aligned} \tag{20}$$

$$\begin{aligned}\mathbf{J}_i \times \mathbf{B}_j = (\ & \{\ (\tfrac{n_i}{R}B_{ri} - \tfrac{\partial B_{zi}}{\partial r})\ B_{zj}\\ & -\ (\tfrac{1}{r}\tfrac{\partial}{\partial r}(rB_{\theta i}) + \tfrac{m_i}{r}B_{ri})\ B_{\theta j}\},\\ & i\{\ (\tfrac{1}{r}\tfrac{\partial}{\partial r}(rB_{\theta i}) + \tfrac{m_i}{r}B_{ri})\ B_{rj}\\ & -\ (\tfrac{m_i}{r}B_{zi} + \tfrac{n_i}{R}B_{\theta i})\ B_{zj}\},\\ & i\{\ (\tfrac{m_i}{r}B_{zi} + \tfrac{n_i}{R}B_{\theta i})\ B_{\theta j}\\ & -\ (\tfrac{n_i}{R}B_{ri} - \tfrac{\partial B_{zi}}{\partial r})\ B_{rj}\}\ )\exp i(m_3\theta - \tfrac{n_3}{R}z),\end{aligned} \tag{21}$$

and

$$
\begin{aligned}
\mathrm{rot}(\mathbf{V}_i \times \mathbf{B}_j) = (\ & i\{ && \tfrac{m_3}{r}\ (\mathrm{V}_{ri}\mathrm{B}_{\theta j} + \mathrm{V}_{\theta i}\mathrm{B}_{rj}) \\
& && -\tfrac{n_3}{R}\ (\mathrm{V}_{zi}\mathrm{B}_{rj} + \mathrm{V}_{ri}\mathrm{B}_{zj})\ \}, \\
& \{ && \tfrac{n_3}{R}\ (\mathrm{V}_{\theta i}\mathrm{B}_{zj} + \mathrm{V}_{zi}\mathrm{B}_{\theta j}) \\
& && -\tfrac{\partial}{\partial r}\ (\mathrm{V}_{ri}\mathrm{B}_{\theta j} + \mathrm{V}_{\theta i}\mathrm{B}_{rj})\ \}, \\
& \{ && -\tfrac{1}{r}\tfrac{\partial}{\partial r} r\ (\mathrm{V}_{zi}\mathrm{B}_{rj} + \mathrm{V}_{ri}\mathrm{B}_{zj}) \\
& && -\tfrac{m_3}{r}\ (\mathrm{V}_{\theta i}\mathrm{B}_{zj} + \mathrm{V}_{zi}\mathrm{B}_{\theta j})\ \})\ \exp i(m_3\theta - \tfrac{n_3}{R}z).
\end{aligned}
\tag{22}
$$

In the equations (18) and (19), we neglect the diffusion terms, since the diffusion terms have no effect to change the phase of the mode. Through these equations the third mode can be expressed by

$$\mathbf{V}_3 = (\mathrm{V}_{r3}, i\mathrm{V}_{\theta 3}, i\mathrm{V}_{z3}) \exp i(m_3\theta - n_3 z/R), \tag{23}$$

$$\mathbf{B}_3 = (i\mathrm{B}_{r3}, \mathrm{B}_{\theta 3}, \mathrm{B}_{z3}) \exp i(m_3\theta - n_3 z/R), \tag{24}$$

where the variables $\mathrm{V}_{\xi 3}$ and $\mathrm{B}_{\xi 3}$ ($\xi = r, \theta$ and z) are real functions. The third mode has the same form as the initial modes. The phase φ of the third mode at the origin is also $\pm 1/2$. Therefore, using the mathematical inductive method, it has been proved that any modes driven nonlinearly have the same phase $\varphi = \pm 1/2$ at the origin.

Acknowledgements

The authors are grateful to Prof. K.Nishikawa for his encouragement through this work. One of them (K.K.) particularly wishes to thank Dr. D.Schnack for the discussion motivating this work. He also wishes to thank Dr. K.Miyamoto, Dr. Z.Yoshida and Dr. C.G.Gimblett for useful discussions.

References

[1] T.Tamano, W.D.Bard, C.Chu, Y.Kondoh, R.J.L.Haye, P.S.Lee, M.Saito, M.J.Schaffer, and P.L.Taylor. *Phys. Rev. Lett.*, 59:1444, 1987.

[2] D.D.Schnack and S.Ortolani. Computational modeling of the effect of a resistive shell on the rfx reversed-field pinch experiment. *Nuclear Fusion*, 30:277, 1990.

[3] K.Kusano and T.Sato. *Nuclear Fusion*, 1990.

[4] D.C.Robinson. Tearing-mode-stable diffuse-pinch configurations. *Nuclear Fusion*, 18:939, 1978.

[5] C.G.Gimblett. On free boundary instabilities induced by a resistive wall. *Nuclear Fusion*, 26:617, 1986.

[6] Y.L.Ho and S.C.Prager. Stability of a reversed field pinch with resistive and distant boundary. *Phys. Fluids*, 31:1673, 1988.

Table I: The modes included in the simulation system.

Case	$m = 0$	$m = 1$
1	n =0 to 20	n =0 to 20
2	n =0 to 20	n =0 to 4, 6 to 20

Figure Caption

FIG. 1. The linear growth rate γ (τ_A^{-1}) of the initial equilibrium for kink ($m = 1; n$) mode is plotted as a function of the toroidal mode number n. The kink modes for $n = 2$ to 9 are unstable.

FIG. 2. The typical toroidal profiles for several quantities are plotted at three different times ($t = 10$, 28 and $40\tau_A$): (a) The normalized mode profiles $\beta(z)$ for the low n ($1 \leq n \leq 10$) kink modes, (b) the dispersion σ for the low n kink modes, (c) the normalized mode profiles $\beta(z)$ for the high n ($11 \leq n \leq 20$) kink modes, (d) the dispersion σ for the high n kink modes, (e) the real profile of $B_r(r = 0.9, \theta = 0, z)$.

FIG. 3. The history of the phase φ_n (a) for the low n ($1 \leq n \leq 10$) kink modes and (b) for the high n ($11 \leq n \leq 20$) kink modes. (c) The history of the spatially minimum dispersion σ for the high n kink modes.

FIG. 4. The relation between the locations $z_{p.l.}$ and z_{n_1/n_2} is plotted by the solid circles for twentysix different runs. (a) $n_1/n_2 = 4/5$ and (b) $n_1/n_2 = 5/6$.

FIG. 5. Time history of the magnetic energy for the initial unstable kink modes ($n = 2$ to 9).

FIG. 6. The histograms of the minimum σ in twenty six runs for (a) Case 1 and (b) Case 2.

FIG. 7. The size of the diamond plotted in the diagram shows the normalized amplitude of the coupling Ξ between the modes $(m; n)$ and $(m'; n')$ at $t = 15\tau_A$.

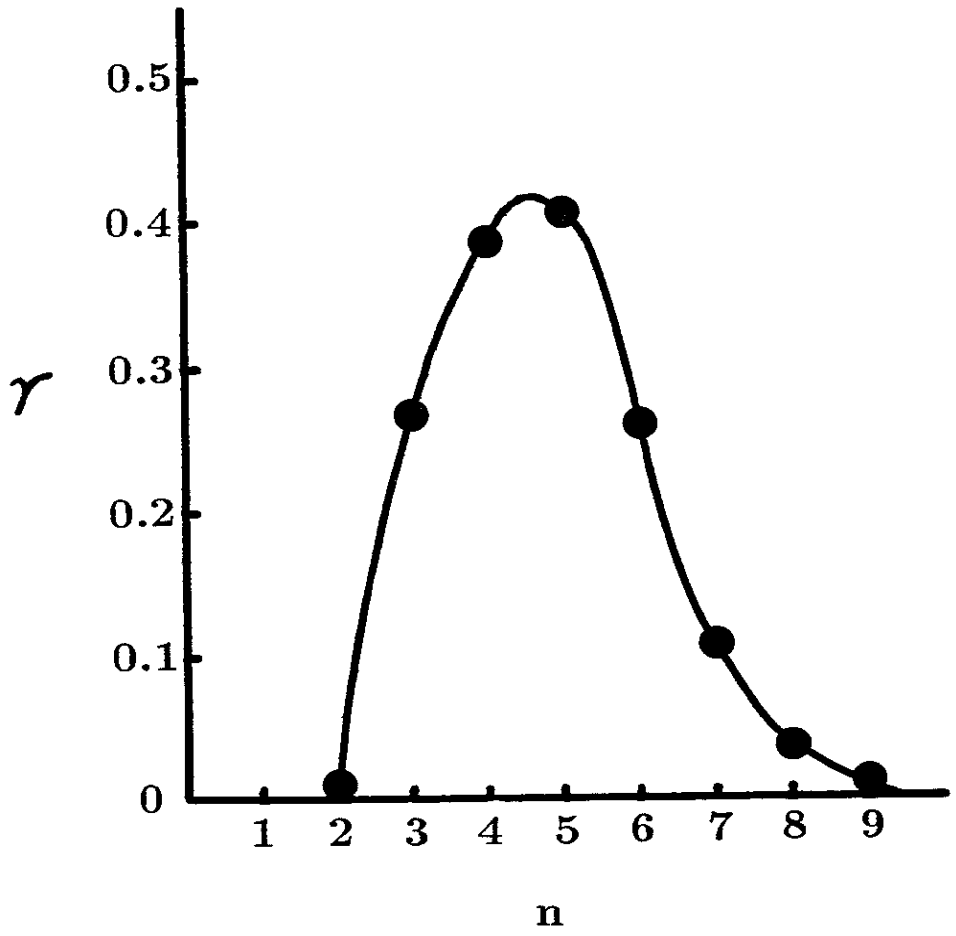

FIG. 1

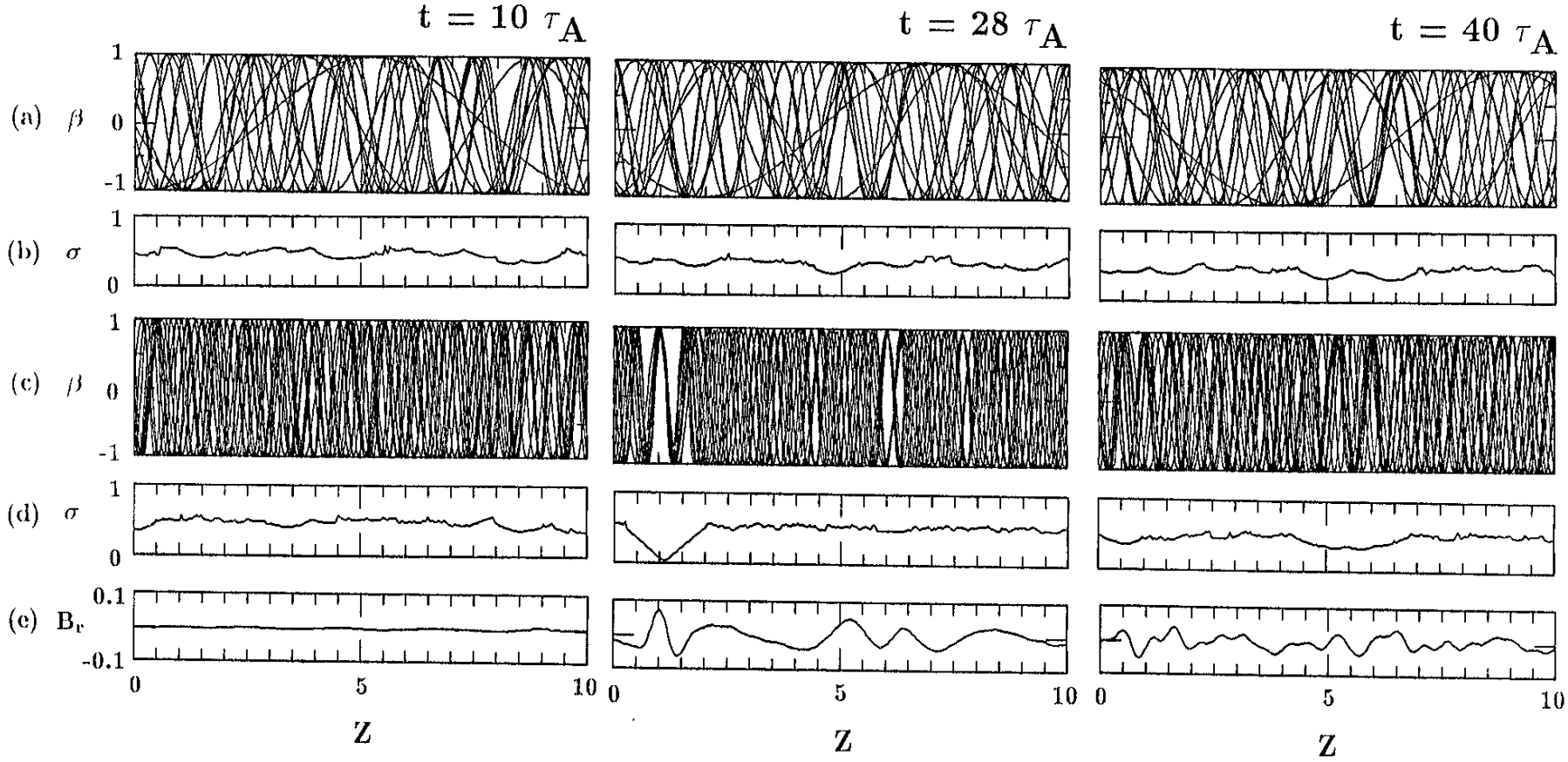
t = 10 τ_A
t = 28 τ_A
t = 40 τ_A
(a) β
(b) σ
(c) β
(d) σ
(e) B_r
1
0
-1
0.1
-0.1
0
5
10
Z

FIG. 2

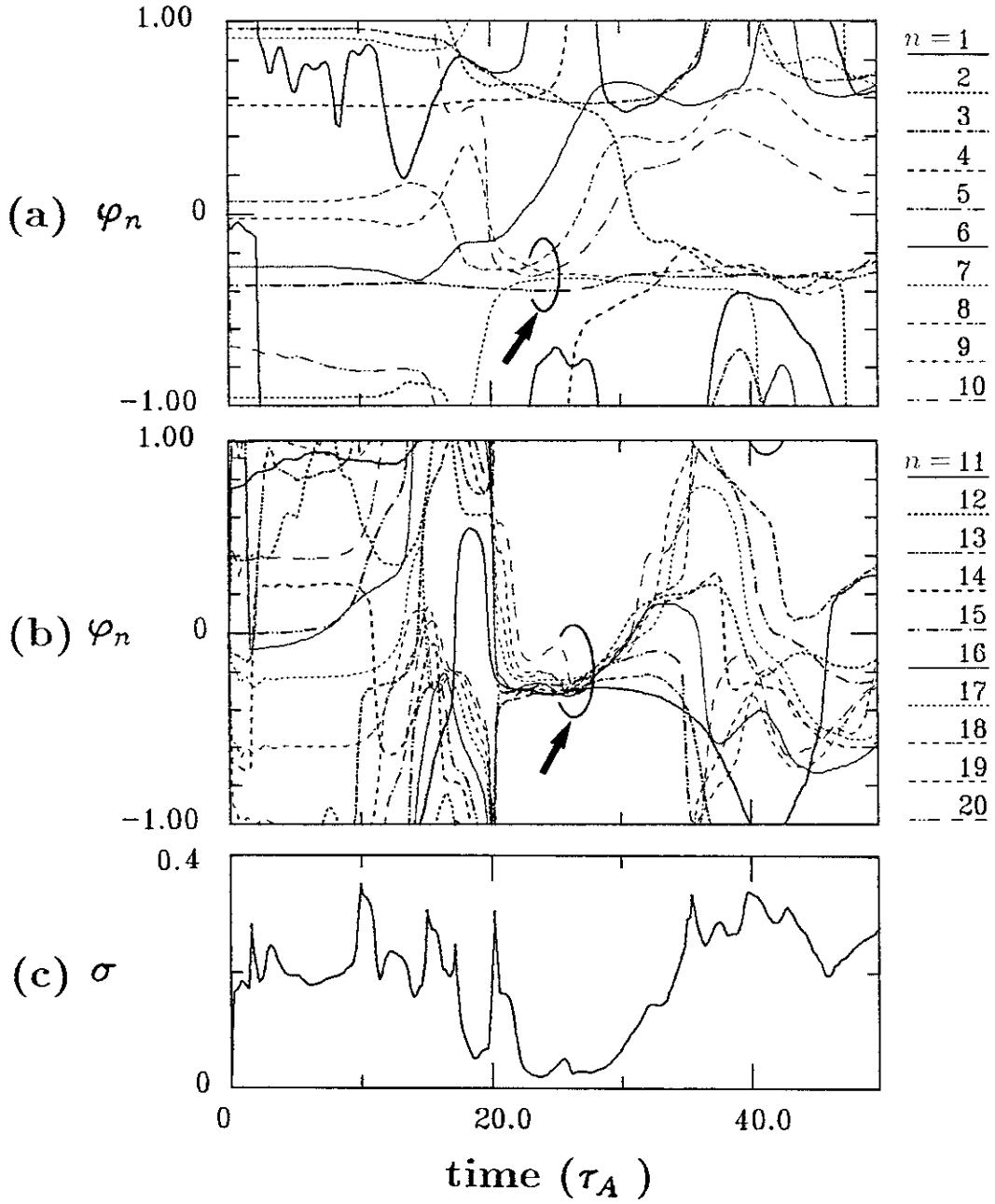
1.00
(a) φ_n
0
−1.00
$n = 1$
2
3
4
5
6
7
8
9
10
1.00
(b) φ_n
0
−1.00
$n = 11$
12
13
14
15
16
17
18
19
20
0.4
(c) σ
0
0
20.0
40.0
time (τ_A)

FIG. 3

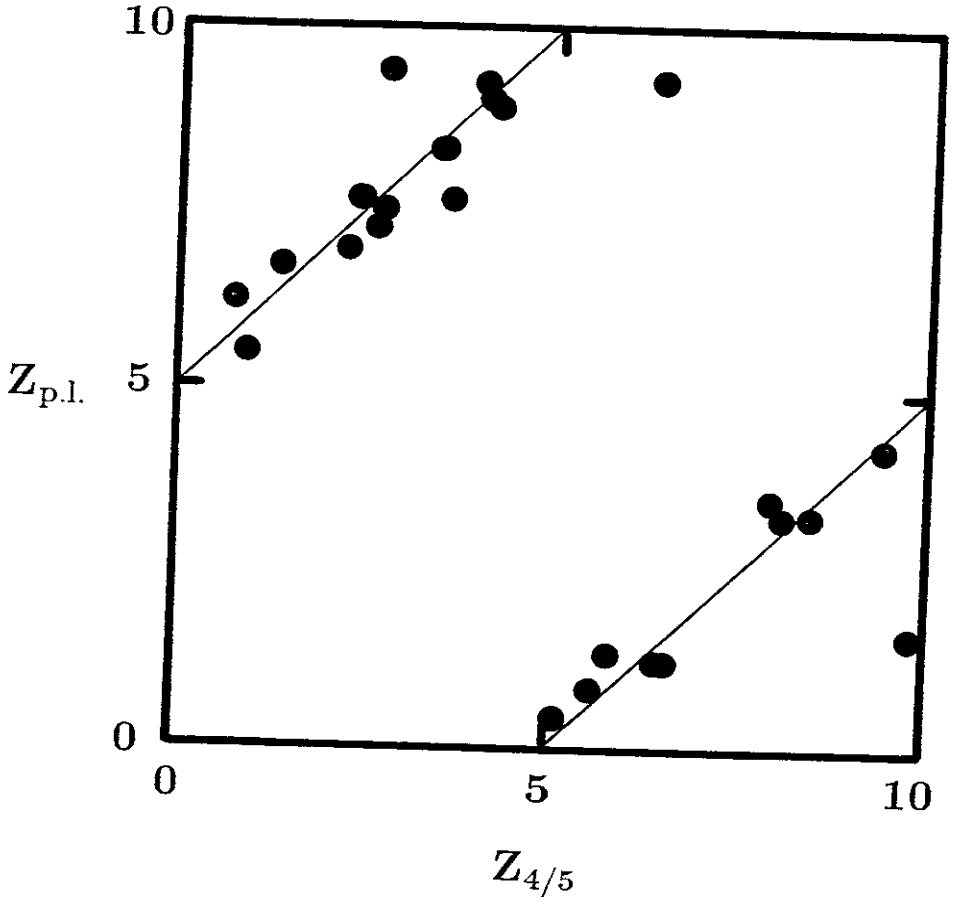

(a)

FIG. 4

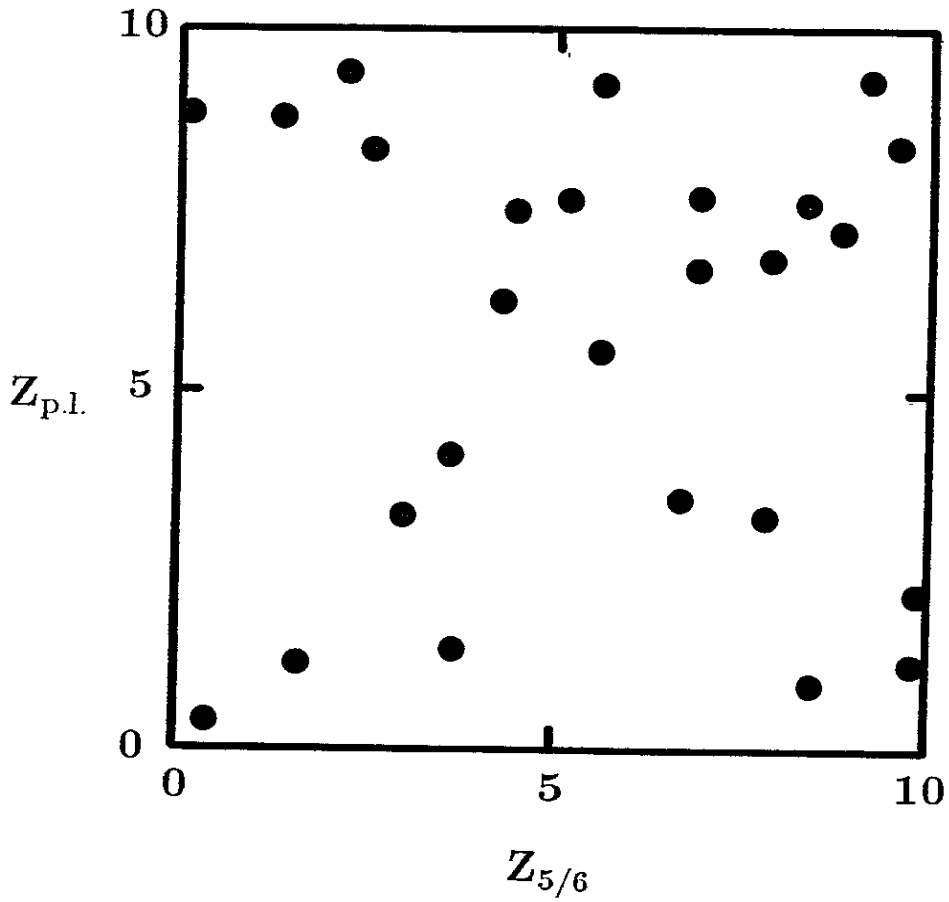

(b)

FIG. 4

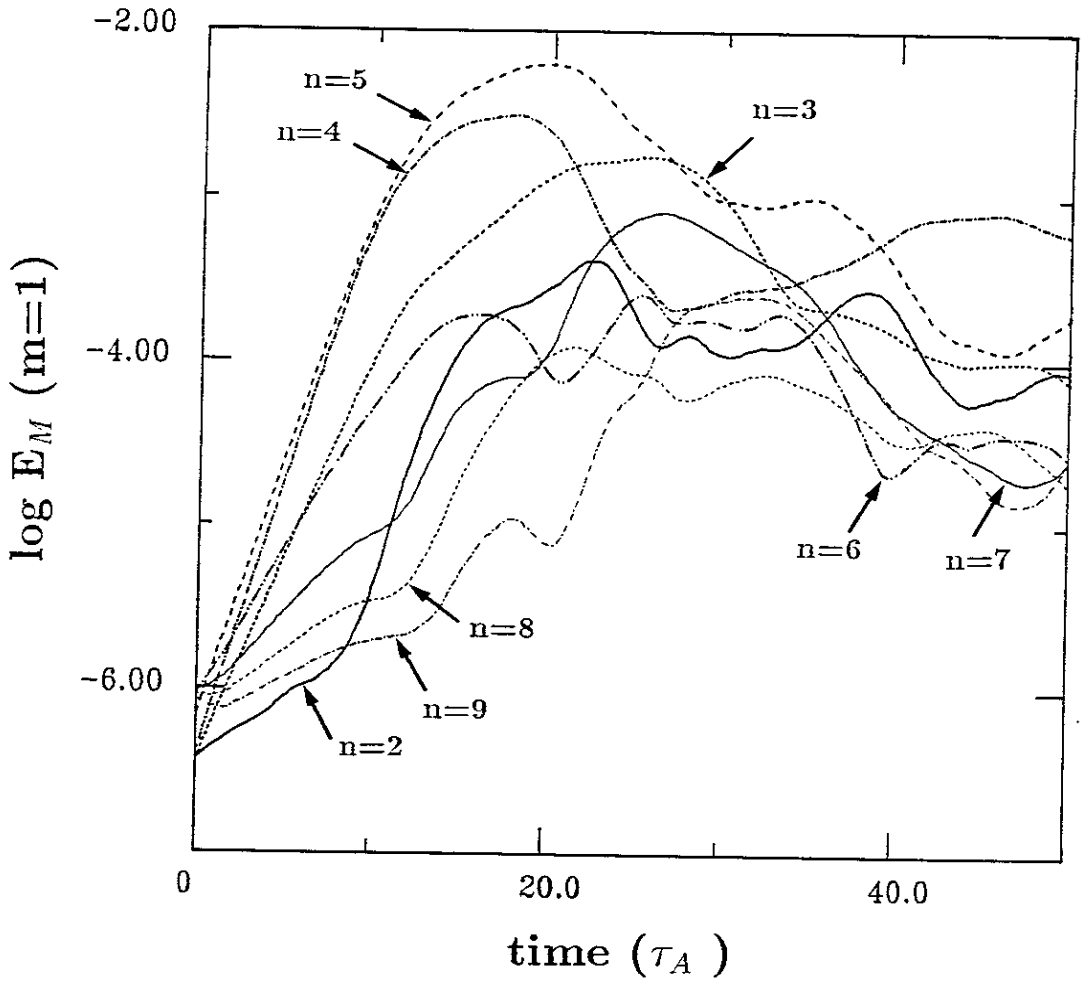

FIG. 5

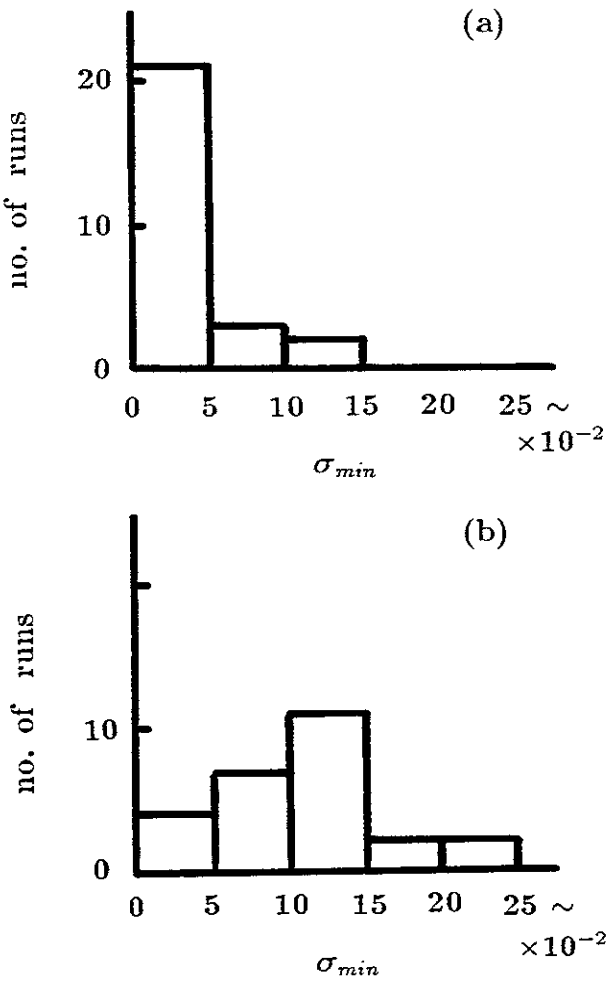
(a)
20
10
0
no. of runs
0
5
10
15
20
25 ~
$\times 10^{-2}$
σ_{min}
(b)
10
0
no. of runs
0
5
10
15
20
25 ~
$\times 10^{-2}$
σ_{min}

FIG. 6

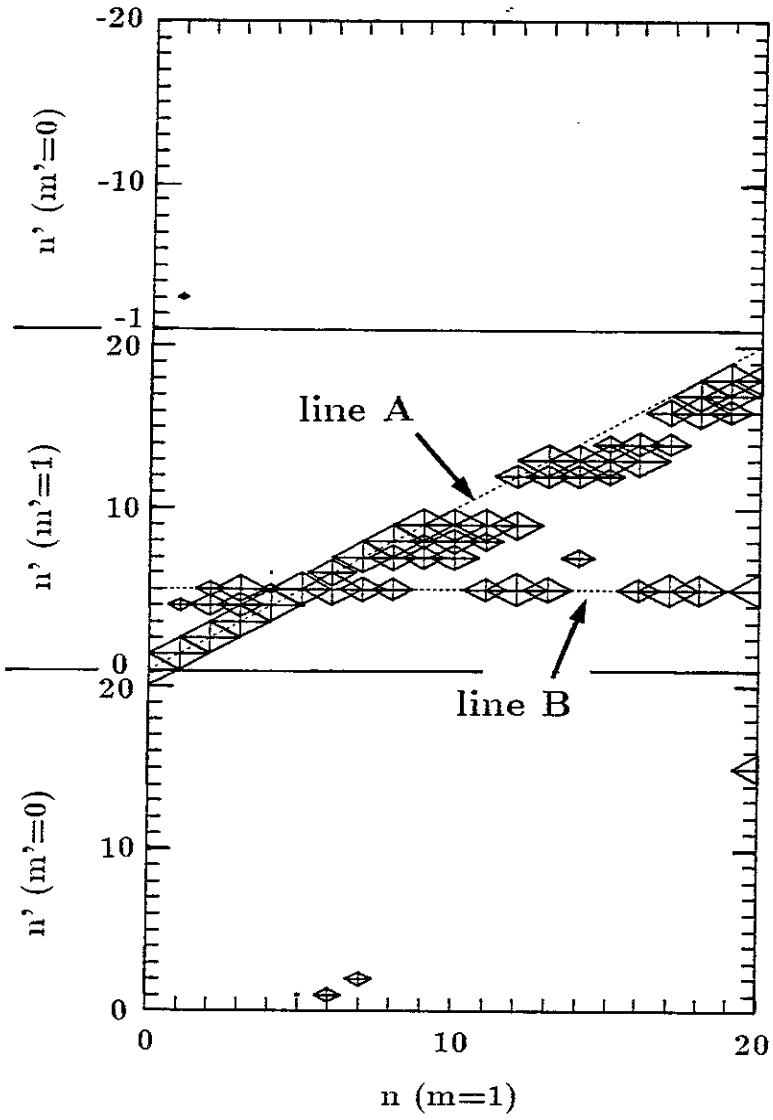

FIG. 7

Recent Issues of NIFS Series

NIFS-27 N. Nakajima and M. Okamoto, *Beam-Driven Currents in the 1/ v Regime in a Helical System* ; Apr. 1990

NIFS-28 K. Itoh, K. Nagasaki and S.I. Itoh, *Heat Deposition on the Partial Limiter* ; Apr. 1990

NIFS-29 S.-I. Itoh A. Fukuyama adn K. Itoh, *Fokker-Plank Equation in the Presence of Anomallous Diffusion* ; May. 1990

NIFS-30 K. Yamazaki, O. Motojima, M. Asao, M. Fujiwara and A. Iiyoshi, *Design Scalings and Optimizations for Super-Conducting Large Helical Devices* ; May 1990

NIFS-31 H. Sanuki, T. Kamimura, K. Hanatani, K. Itoh and J. Todoroki, *Effects of Electric Field on Particle Drift Orbits in a l =2 Torsatron* ; May 1990

NIFS-32 Yoshi H. Ichikawa, *Experiments and Applications of Soliton Physics*; June 1990

NIFS-33 S.-I. Itoh, *Anomalous Viscosity due to Drift Wave Turbulence* ; June 1990

NIFS-34 K. Hamamatsu, A. Fukuyama, S.-I. Itoh, K. Itoh and M. Azumi, *RF Helicity Injection and Current Drive* ; July 1990

NIFS-35 M. Sasao, H. Yamaoka, M. Wada and J. Fujita, *Direct Extraction of a Na- Beam from a Sodium Plasma* ; July 1990

NIFS-36 N. Ueda, S.-I. Itoh, M. Tanaka and K. Itoh, *A Design Method of Divertor in Tokamak Reactors* Aug. 1990

NIFS-37 J. Todoroki, *Theory of Longitudinal Adiabatic Invariant in the Helical Torus*; Aug. 1990

NIFS-38 S.-I. Itoh and K. Itoh, *Modelling of Improved Confinements – Peaked Profile Modes and H-Mode–* ; Sep. 1990

NIFS-39 O. Kaneko, S. Kubo, K. Nishimura, T. Syoji, M. Hosokawa, K. Ida, H. Idei, H. Iguchi, K. Matsuoka, S. Morita, N. Noda, S. Okamura, T. Ozaki, A. Sagara, H. Sanuki, C. Takahashi, Y. Takeiri, Y. Takita, K. Tsuzuki, H. Yamada, T. Amano, A. Ando, M. Fujiwara, K. Hanatani, A. Karita, T. Kohmoto, A. Komori, K. Masai, T. Morisaki, O. Motojima, N. Nakajima, Y. Oka, M. Okamoto, S. Sobhanian and J. Todoroki, *Confinement Characteristics of High Power Heated Plasma in CHS*; Sep. 1990

NIFS-40 K. Toi, Y. Hamada, K. Kawahata, T. Watari, A. Ando, K. Ida, S. Morita, R. Kumazawa, Y. Oka, K. Masai, M. Sakamoto, K. Adati, R. Akiyama, S. Hidekuma, S. Hirokura, O. Kaneko, A. Karita, T. Kawamoto, Y. Kawasumi, M. Kojima, T. Kuroda, K. Narihara, Y. Ogawa, K. Ohkubo, S. Okajima, T. Ozaki, M. Sasao, K. Sato, K.N. Sato, T. Seki, F. Shimpo, H. Takahashi, S. Tanahashi, Y. Taniguchi and T. Tsuzuki, *Study of Limiter H- and IOC- Modes by Control of Edge Magnetic Shear and Gas Puffing in the JIPP T-IIU Tokamak*; Sep. 1990

NIFS-41 K. Ida, K. Itoh, S.-I. Itoh, S. Hidekuma and JIPP T-IIU & CHS Group, *Comparison of Toroidal/Poloidal Rotation in CHS Heliotron/Torsatron and JIPP T-IIU Tokamak*; Sep .1990

NIFS-42 T.Watari, R.Kumazawa,T.Seki, A.Ando,Y.Oka, O.Kaneko, K.Adati, R.Ando, T.Aoki, R.Akiyama, Y.Hamada, S.Hidekuma, S.Hirokura, E.Kako, A.Karita, K.Kawahata, T.Kawamoto, Y.Kawasumi, S.Kitagawa, Y.Kitoh, M.Kojima, T. Kuroda, K.Masai, S.Morita, K.Narihara, Y.Ogawa, K.Ohkubo, S.Okajima, T.Ozaki, M.Sakamoto, M.Sasao, K.Sato, K.N.Sato, F.Shinbo, H.Takahashi, S.Tanahashi, Y.Taniguchi, K.Toi, T.Tsuzuki, Y.Takase, K.Yoshioka, S.Kinoshita, M.Abe, H.Fukumoto, K.Takeuchi, T.Okazaki and M.Ohtuka, *,Application of Intermediate Frequency Range Fast Wave to JIPP T-IIU and HT-2 Plasma*; Sep. 1990

NIFS-43 K.Yamazaki, N.Ohyabu, M.Okamoto, T.Amano, J.Todoroki, Y.Ogawa, N.Nakajima, H.Akao, M.Asao, J.Fujita, Y.Hamada, T.Hayashi, T.Kamimura, H.Kaneko, T.Kuroda, S.Morimoto, N.Noda, T.Obiki, H.Sanuki, T.Sato, T.Satow, M.Wakatani, T.Watanabe, J.Yamamoto, O.Motojima, M.Fujiwara, A.Iiyoshi and LHD Design Group, *Physics Studies on Helical Confinement Configurations with l=2 Continuous Coil Systems*; Sep. 1990

NIFS-44 T.Hayashi, A.Takei, N.Ohyabu, T.Sato, M.Wakatani, H.Sugama, M.Yagi, K.Watanabe, B.G.Hong and W.Horton, *Equilibrium Beta Limit and Anomalous Transport Studies of Helical Systems*; Sep. 1990

NIFS-45 R.Horiuchi, T.Sato, and M.Tanaka, *Three-Dimensional Particle Simulation Study on Stabilization of the FRC Tilting Instability*; Sep. 1990

NIFS-46 K.Kusano, T.Tamano and T. Sato, *Simulation Study of Nonlinear Dynamics in Reversed-Field Pinch Configuration*; Sep. 1990

NIFS-47 Yoshi H.Ichikawa, *Solitons and Chaos in Plasma*; Sep. 1990

NIFS-48 T.Seki, R.Kumazawa, Y.Takase, A.Fukuyama, T.Watari, A.Ando, Y.Oka, O.Kaneko, K.Adati, R.Akiyama, R.Ando, T.Aoki, Y.Hamada, S.Hidekuma, S.Hirokura, K.Ida, K.Itoh, S.-I.Itoh, E.Kako, A. Karita, K.Kawahata, T.Kawamoto, Y.Kawasumi, S.Kitagawa, Y.Kitoh,

M.Kojima, T.Kuroda, K.Masai, S.Morita, K.Narihara, Y.Ogawa, K.Ohkubo, S.Okajima, T.Ozaki, M.Sakamoto, M.Sasao, K.Sato, K.N.Sato, F.Shinbo, H.Takahashi, S.Tanahashi, Y.Taniguchi, K.Toi and T.Tsuzuki, *Application of Intermediate Frequency Range Fast Wave to JIPP T-IIU Plasma*; Sep.1990

NIFS-49 A.Kageyama, K.Watanabe and T.Sato, *Global Simulation of the Magnetosphere with a Long Tail: The Formation and Ejection of Plasmoids*; Sep.1990

NIFS-50 S.Koide, *3-Dimensional Simulation of Dynamo Effect of Reversed Field Pinch*; Sep. 1990

NIFS-51 O.Motojima, K. Akaishi, M.Asao, K.Fujii, J.Fujita, T.Hino, Y.Hamada, H.Kaneko, S.Kitagawa, Y.Kubota, T.Kuroda, T.Mito, S.Morimoto, N.Noda, Y.Ogawa, I.Ohtake, N.Ohyabu, A.Sagara, T. Satow, K.Takahata, M.Takeo, S.Tanahashi, T.Tsuzuki, S.Yamada, J.Yamamoto, K.Yamazaki, N.Yanagi, H.Yonezu, M.Fujiwara, A.Iiyoshi and LHD Design Group, *Engineering Design Study of Superconducting Large Helical Device*; Sep. 1990

NIFS-52 T.Sato, R.Horiuchi, K. Watanabe, T. Hayashi and K.Kusano, *Self-Organizing Magnetohydrodynamic Plasma*; Sep. 1990

NIFS-53 M.Okamoto and N.Nakajima, *Bootstrap Currents in Stellarators and Tokamaks*; Sep. 1990

NIFS-54 K.Itoh and S.-I.Itoh, *Peaked-Density Profile Mode and Improved Confinement in Helical Systems*; Oct. 1990

NIFS-55 Y.Ueda, T.Enomoto and H.B.Stewart, *Chaotic Transients and Fractal Structures Governing Coupled Swing Dynamics*; Oct. 1990

NIFS-56 H.B.Stewart and Y.Ueda, *Catastrophes with Indeterminate Outcome*; Oct. 1990

NIFS-57 S.-I.Itoh, H.Maeda and Y.Miura, *Improved Modes and the Evaluation of Confinement Improvement*; Oct. 1990

NIFS-58 H.Maeda and S.-I.Itoh, *The Significance of Medium- or Small-size Devices in Fusion Research*; Oct. 1990

NIFS-59 A.Fukuyama, S.-I.Itoh, K.Itoh, K.Hamamatsu, V.S.Chan, S.C.Chiu, R.L.Miller and T.Ohkawa, *Nonresonant Current Drive by RF Helicity Injection*; Oct. 1990

NIFS-60 K.Ida, H.Yamada, H.Iguchi, S.Hidekuma, H.Sanuki, K.Yamazaki and CHS Group, *Electric Field Profile of CHS Heliotron/Torsatron Plasma with Tangential Neutral Beam Injection*; Oct. 1990

NIFS-61 T.Yabe and H.Hoshino, *Two- and Three-Dimensional Behavior of Rayleigh-Taylor and Kelvin-Helmholz Instabilities*; Oct. 1990

NIFS-62 H.B. Stewart, *Application of Fixed Point Theory to Chaotic Attractors of Forced Oscillators;* Nov. 1990

NIFS-63 K.Konn., M.Mituhashi, Yoshi H.Ichikawa,*Soliton on Thin Vortex Filament;* Dec. 1990

NIFS-64 K.Itoh, S.-I.Itoh and A.Fukuyama,*Impact of Improved Confinement on Fusion Research;* Dec. 1990

NIFS -65 A.Fukuyama, S.-I.Itoh and K. Itoh,*A Consistency Analysis on the Tokamak Reactor Plasmas;* Dec. 1990

NIFS-66 K.Itoh, H. Sanuki, S.-I. Itoh and K. Tani,*Effect of Radial Electric Field on α-Particle Loss in Tokamaks;* Dec. 1990

NIFS-67 K.Sato,and F.Miyawaki,*Effects of a Nonuniform Open Magnetic Field on the Plasma Presheath*; Jan.1991

NIFS-68 K.Itoh and S.-I.Itoh,*On Relation between Local Transport Coefficient and Global Confinement Scaling Law;* Jan. 1991

NIFS-69 T.Kato, K.Masai, T.Fujimoto,F.Koike, E.Källne, E.S.Marmar and J.E.Rice,*He-like Spectra Through Charge Exchange Processes in Tokamak Plasmas;* Jan.1991

NIFS-70 K. Ida, H. Yamada, H. Iguchi, K. Itoh and CHS Group, *Observation of Parallel Viscosity in the CHS Heliotron/Torsatron* ; Jan.1991

NIFS-71 H. Kaneko, *Spectral Analysis of the Heliotron Field with the Toroidal Harmonic Function in a Study of the Structure of Built-in Divertor* ; Jan. 1991

NIFS-72 S. -I. Itoh, H. Sanuki and K. Itoh, *Effect of Electric Field Inhomogeneities on Drift Wave Instabilities and Anomalous Transport* ; Jan. 1991

NIFS-73 Y.Nomura, Yoshi.H.Ichikawa and W.Horton,*Stabilities of Regular Motion in the Relativistic Standard Map;* Feb. 1991

NIFS-74 T.Yamagishi, *;Electrostatic Drift Mode in Toroidal Plasma with Minority Energetic Particles,* Feb. 1991

NIFS-75 T.Yamagishi, *Effect of Energetic Particle Distribution on Bounce Resonance Excitation of the Ideal Ballooning Mode,* Feb. 1991

NIFS-76 T.Hayashi, A.Takei, N.Ohybu, T.Sato, *Suppression of Magnetic Surface Breaking by Simple Extra Coils in Finite Beta Equilibrium of Helical System*; Feb. 1991

NIFS-77 N.Ohyabu, *High Temperature Divertor Plasma Operation;* Feb. 1991